Investigation on hot cracking during laser welding by means of experimental and numerical methods

Gao, He; Agarwal, Gautam; Amirthalingam, Muru; Hermans, Marcel; Richardson, Ian

DOI
10.1007/s40194-017-0524-z

Publication date
2018

Document Version
Final published version

Published in
Welding in the World

Welding in the World (2018) 62:71–78
https://doi.org/10.1007/s40194-017-0524-z

RESEARCH PAPER

Investigation on hot cracking during laser welding by means of experimental and numerical methods

H. Gao[1] · G. Agarwal[1] · M. Amirthalingam[2] · M. J. M. Hermans[1] · I. M. Richardson[1]

Received: 4 August 2017 / Accepted: 10 November 2017 / Published online: 4 December 2017

Abstract
Hot cracking during laser welding of Transformation Induce Plasticity (TRIP) steel at the edges of steel flanges can be a problem. In this study, modified hot cracking tests were performed by welding on a single-side clamped specimen at various distances from the free edge, while the heat input and external constraints remained constant. In situ temperature and strain measurements were carried out using pre-attached thermocouples and digital image correlation, respectively. A thermal-mechanical finite element (FE) model was constructed and validated with the temporal and spatial data measured. From the validated FE model, the temperature and strain evolution in the weld mushy zone were studied. A critical strain for the onset of hot cracking in the TRIP steel examined was found to be in the range of 3.2 to 3.6%. This threshold was further evaluated and experimentally confirmed by welding with different heat inputs.

Keywords Hot cracking · Laser welding · Digital image correlation · Finite element model · Temporal and spatial validation

1 Introduction

Advanced high-strength steels (AHSS) are increasingly applied by automotive manufacturers [1], which can reduce the car weight by using high-strength thinner gauge steel sheets. Application of laser welding at the edges of steel flanges is often required [2]; however, hot cracking of laser welded components in certain AHSS steel grades can be an issue associated with such a weld geometry [3].

In order to obtain the desired mechanical properties in AHSS, alloying elements and complex heat treatments are applied to generate microstructures with designed fractions, dimensions, compositions, morphologies, and spatial distribution of phases [4, 5]. However, the solidification range of the materials can be broadened by adding the alloying elements, and thus, the hot cracking susceptibility is increased. The metallurgical and thermal-mechanical conditions during solidification are crucial for hot cracking [6]. The occurrence of hot cracking has been studied on different length scales. On the microscale level, Rappaz [7] proposes that a hot tear between columnar dendrites is formed as a result of a localized strain transmitted by the coherent dendrites. Kou [8] states that hot cracking is caused by tensile deformation induced in the semi-solid region along grain boundaries when liquid is not sufficiently fed. Wang [9] concludes that the segregation and morphology of liquid channels in the last stages of solidification make materials more susceptible to hot cracking. Coniglio [10] describes the crack initiation and growth mechanisms during welding solidification in terms of critical stress to fracture the inter-dendritic liquid, critical strain to exceed the mushy zone ductility and critical hydrogen content to nucleate and grow a pore. On the macroscale level, welding processes induce a thermal load and mechanical deformation. During cooling, the solidifying melt contracts due to both solidification shrinkage and thermal contraction. Prokhorov [11] proposes a hot tearing criterion based on the material ductility and deformation of the liquid-solid region. Clyne [12] describes a hot cracking index by evaluating the cooling rate in the material solidification range. Yamanaka [13] determines a critical value for cracking when the inelastic strain in the mushy zone exceeds this value. Won [14] suggests an empirical relation for critical strain considering the strain rate in the brittle temperature range and the material properties.

Recommended for publication by Commission IX - Behavior of Metals Subjected to Welding

✉ H. Gao
H.Gao@tudelft.nl

[1] Materials Science and Engineering Department, Delft University of Technology, Mekelweg 2, 2628 CD Delft, The Netherlands

[2] Department of Metallurgical and Materials Engineering, Indian Institute of Technology Madras, Chennai 600036, India

Simulations of hot cracking phenomena are widely conducted via multi-physics and multi-scale approaches. Safari [15] implements a visco-plastic constitutive model into a finite element simulation. A maximum transverse mechanical strain criterion for both initiation and propagation of hot cracking is determined. Wang [16] creates a sequentially coupled model, where the welding thermal and mechanical boundary conditions are translated into a microstructure domain. A critical pressure drop in the inter-dendritic region for hot cracking is obtained. Ploshikhin [17] presents an integrated mechanical-metallurgical approach to simulate the solidification cracking in welds. Hot cracking is found as a result of accumulation of macroscopic tensile strains in a microscopic intergranular film of liquid. In general, most numerical models are only validated with in situ temperature measurements, while the stress/strain fields are derived from coupled thermal-mechanical simulations. Hot cracking is a dynamic process, and a reliable hot cracking criterion should therefore be determined based on numerical models validated with in situ temporal and spatial stress/strain measurements adjacent to the fusion boundary.

In this study, laser welding was performed at various distances from the free edge of a steel coupon based on a modified hot cracking test. In situ temperature and strain measurements were carried out using pre-attached thermocouples and digital image correlation, respectively. The measured transient results provide vital information to validate relevant numerical models. From the validated FE model, the evolution of the isothermal surface and transverse strain in the weld mushy zone were studied. By comparing two cases with and without hot cracks, a critical strain during solidification is determined, which is proven to be a successful threshold in predicting the occurrence of hot cracking.

2 Experiments

A standard self-restraint hot cracking test developed by the VDEh (German Steel Institute) [18] is normally used by European steelmakers to test the resistance of an automotive steel to solidification cracking. Laser bead-on-plate welding is carried out on rectangular steel sheets at an inclination of 7° to the edge with a starting distance of 3 mm from the free edge. The other edge is fixed by clamps as shown in Fig. 1a. The length of a crack is used as a parameter to rank the hot cracking susceptibilities of various steel grades. However, the amount of restraint is gradually increased as the laser travels into the sheet with an inclined angle. It is very difficult to determine a critical strain that initiates hot cracking due to the self-restraints. Therefore, a modified hot cracking test was designed as shown in Fig. 1b. Laser welding was carried out at increasing distances parallel to the free edge.

The bead-on-plate welding experiments were performed using a 3 kW Nd:YAG laser with a power of 1100 W and welding speed of 10 mm s^{-1}. Rectangular steel sheets of dimensions 90 × 45 mm^2 and a thickness of 1.25 mm were used. Transformation induced plasticity (TRIP) steel with chemical composition listed in Table 1 is examined in this work. The distance of the laser beam from the free edge was increased until no cracking was observed; this occurred at a distance of 13 mm. For each of the welding case, experiments were repeated five times. Transient temperature was measured by spot-welded K-type thermocouples with a diameter of 0.25 mm at three positions in the heat-affected-zone (HAZ) as shown in Fig. 1c.

A random speckle pattern was made on the top side of the steel sheet using a commercial high-temperature paint. The speckle pattern size is measured and varies from 10 to 50 μm. A LIMESS™ Q-400-3D digital image correlation (DIC) system along with the commercial software Istra 4D was used to capture and analyze images at a frame rate of 8 Hz [19]. From the DIC system, the motion of the speckle pattern is used to derive the displacement and strain. In order to minimize the intensity of the generated weld plume, two customized auxiliary high-intensity 30 W LEDs with wavelength 450 nm were used to illuminate the top surface of the

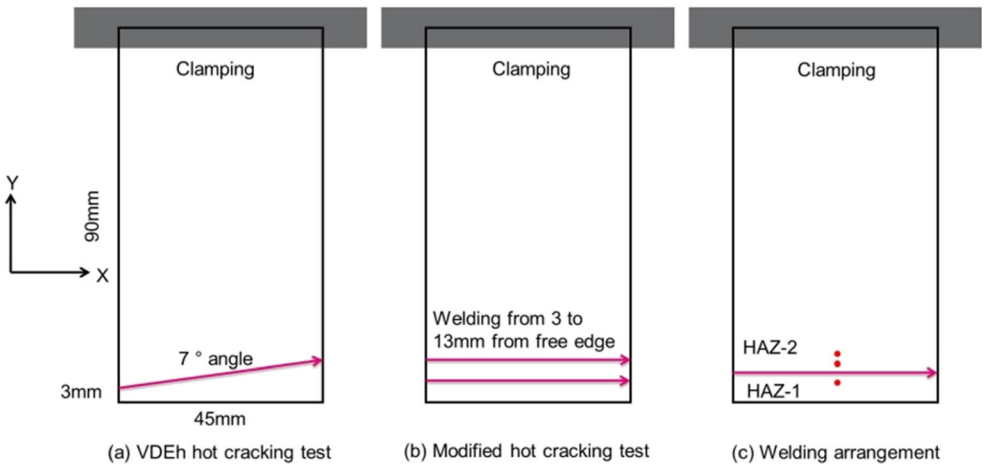

Fig. 1 Schematic top view of **a** standard self-restraint hot cracking test (VDEh), the red line indicates the weld center line; **b** modified hot cracking test at increasing distances parallel to the free edge; and **c** welding arrangement in this study: transient temperature is measured in HAZ-1 at 3 mm from the weld center line and HAZ-2 at 2.5 and 4 mm from the weld center line

Table 1 Chemical compositions of TRIP steel (in wt%, with Fe balance)

	C	Mn	Si	Cr	P	Al
TRIP	0.19	1.63	0.35	0.019	0.089	1.1

specimen. A corresponding optical bandpass filter with a center wavelength of 450 nm and a full width half maximum (FWHM) of 10 nm were placed in front of the lenses to minimize the effect of the plume light. This approach allowed measurement of the displacement fields as close as 1.5 to 2 mm from the fusion boundary. The maximum strain uncertainty close to the fusion boundary is ± 0.1% in this work.

3 Finite element model

A sequentially coupled 3D finite element (FE) thermal-mechanical model was constructed to include the physics of heat transfer and solid mechanics [20]. The commercial software, COMSOL™ was used for this purpose. The heat balance during welding was simulated including the heat input, heat transfer, and heat loss. The heat input was applied as a volumetric conical heat source with Gaussian distribution as shown in Fig. 2c. The heat transfer in the sheet was determined by the temperature-dependent thermal properties as shown in Fig. 2a [21]. The latent heats due to phase transformations were included in the specific heat. The heat loss was modeled via a surface film boundary condition. Room temperature was considered as a reference temperature.

The thermal history obtained was applied as a predefined field to the mechanical model. Fixed constraints were applied to simulate the clamping condition. An elasto-plastic theory with isotropic hardening was used [22]. Green-Lagrange and second Piola-Kirchhoff theories were assumed in the FE model to calculate strain and stress. The volume change due to solid-liquid phase transformation was included in the thermal expansion coefficient. The temperature-dependent mechanical and material properties are given in Fig. 2b [21]. The solid state phase transformation is neglected, as the focus of this work is to determine the critical strain at high temperature in the weld mushy zone. The mesh setup near the weld center line is denser ($0.5 \times 0.5 \times 0.5$ mm^3) compared to the base materials as shown in Fig.2d.

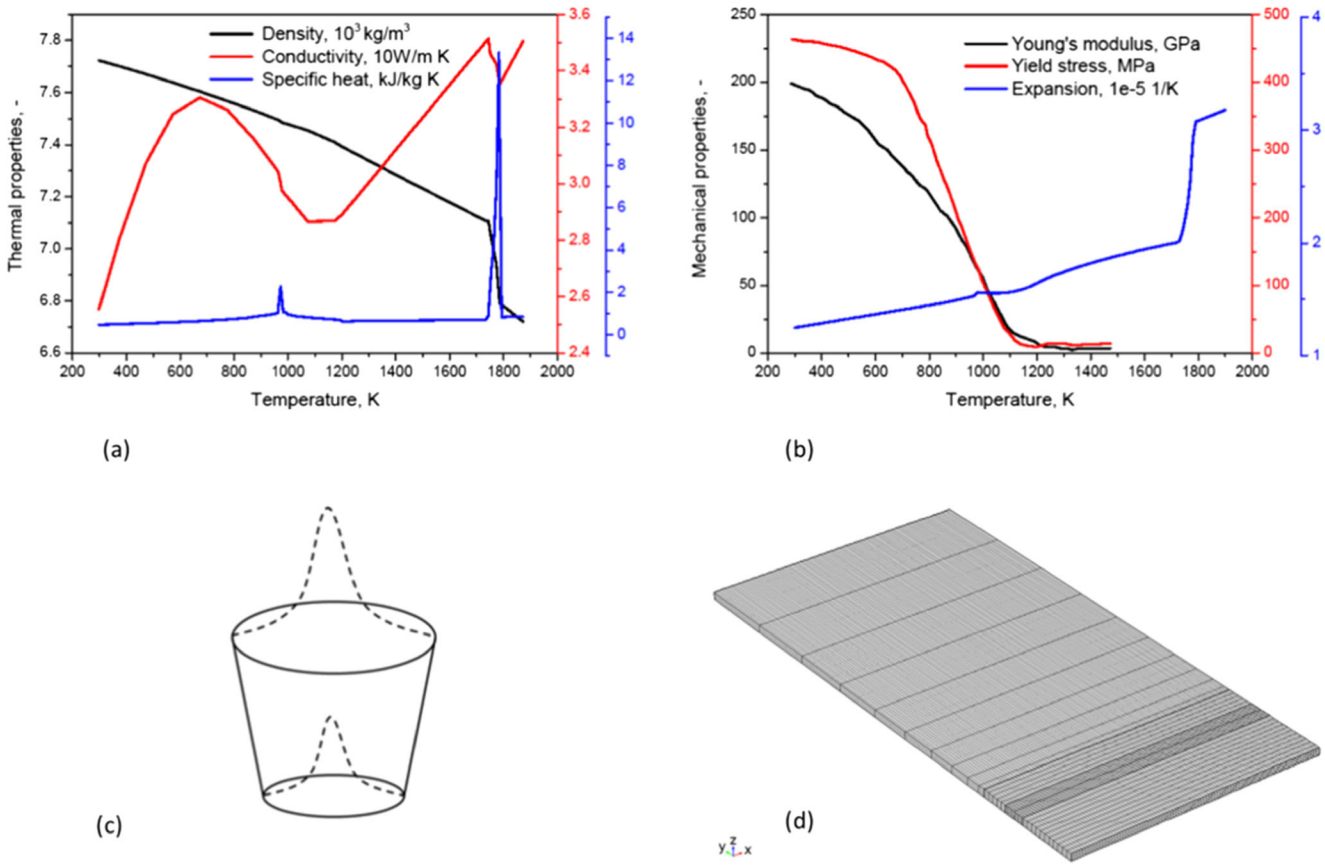

Fig. 2 FE model set-up: **a** temperature dependent thermal properties, **b** temperature-dependent mechanical properties, **c** conical heat source, **d** model mesh

4 Results

Laser welding was performed at 11 and 13 mm from the free edge of the steel coupons. Full penetration was obtained for both of the cases. After welding, cracks were observed along the weld center line on all samples when welding at 11 mm from the free edge, whereas no cracks were observed when welding at 13 mm from the free edge as shown in Fig. 3.

Figure 4 shows the experimental and numerical results of the transient temperature at three locations in the heat-affected zone, when welding at 13 mm from the free edge. The red curve represents the temperature at 2.5 mm from the weld center line in HAZ2 and shows a peak temperature of 1025 K. The black curve represents the temperature at 3 mm from the weld center line in HAZ1 and shows a lower peak temperature of 940 K. During the subsequent cooling stage, the curves of these two locations intersect due to asymmetrical heat dissipation. The blue curve represents the temperature at 4 mm from the weld center line in HAZ2, which shows the lowest peak temperature of 830 K of the three locations measured. Good agreement was found between the experimental and numerical results with respect to peak temperatures and temperature profiles in the heating and cooling stages at these three locations.

The experimental and numerical transverse strains in HAZ1 at 3 mm from the weld center line in the middle of the weld sheet (22.5 mm from the starting edge) are shown in Fig. 5. The strains at the free edge in the middle of the weld sheet are shown in Fig. 6. Good agreements of strain evolution between experiments and simulations at these two locations are indicated. The strain in the HAZ1 increases up to 1% during the heating stage and then decreases to 0.4% upon cooling at a time of 30 s after welding started. At the free edge, the strain reaches 0.6% and decreases slowly.

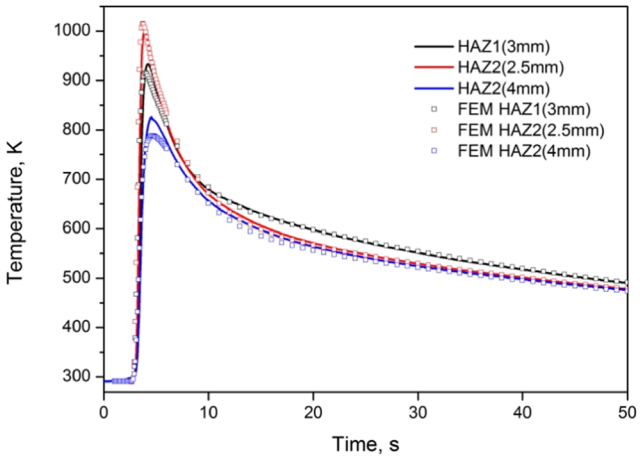

Fig. 4 Experimental and numerical results of the transient temperature in HAZ1 at 3 mm and HAZ2 at 2.5 and 4 mm from the weld center line in the middle of the weld sheet (22.5 mm from the starting edge) when welding at 13 mm from the free edge

Transverse strain maps obtained from experiment and FE model are compared at time $t = 3.5$ s after the start of welding and are shown in Fig. 7. The spatial strains are compared over an area of 45×10 mm^2. The FE model predicts the strain range and distribution and shows a good match to the measured results.

5 Discussion

The heat input and clamping condition were kept the same when welding at 13 and 11 mm from the free edge, while a

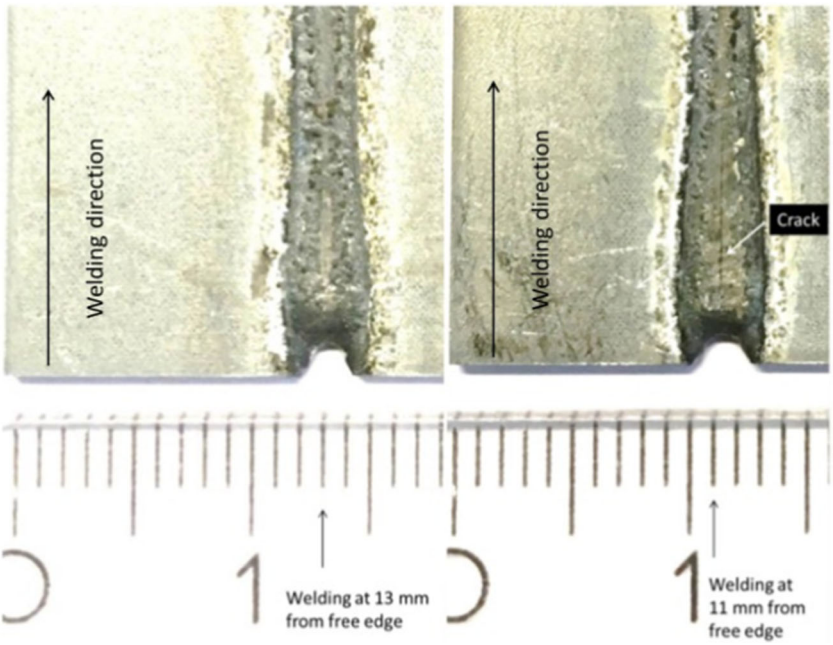

Fig. 3 Sheets laser welded at 13 and 11 mm from the free edge

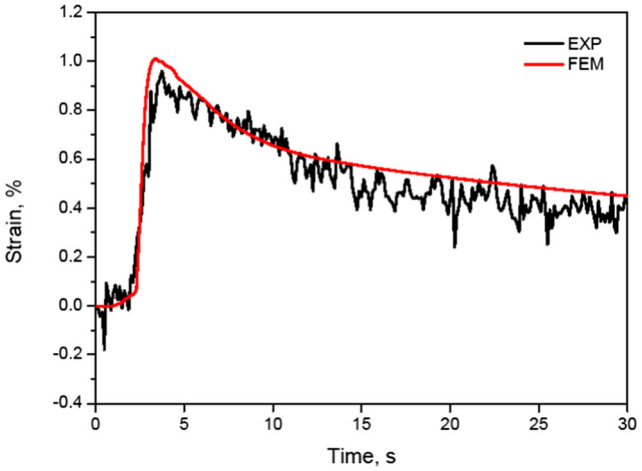

Fig. 5 Strain validation in HAZ1 at 3.5 mm from the weld center line in the middle of the weld sheet when welding at 13 mm from the free edge

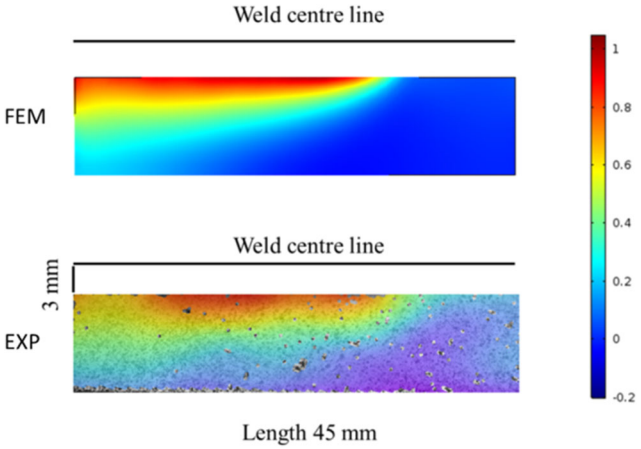

Fig. 7 Strain (%) map validation when $t = 3.5$ s after the start of welding

crack is only observed in the latter case. This implies that the crack initiation is related to the self-restraints of the material and the strain built-up in the weld center during solidification.

Although the strain distribution and evolution during welding were measured by DIC, the measurements can only be executed at a distance greater than 3 mm from the weld center line on the top surface, as the paint of the random speckle pattern is not able to withstand temperatures beyond 1300 K. However, the crack occurs in the center of the weld during welding, which indicates that the temperature and strain evolution in the weld mushy zone are essential to explain the hot cracking susceptibility. The transient temperature and strain measured outside of the weld mushy zone are used to compare with the results predicted from the FE model. After the FE model was validated with the temporal and spatial data, the temperature and strain distribution and evolution on the weld center can be extracted.

Figure 8 shows the simulated temperature evolution at the starting edge in the weld center and at the free edge when welding at 13 and 11 mm from the free edge. As the heat source is locally applied at the weld center, the temperature profiles in the fusion zone are similar and overlap each other. It can be seen that the peak temperature for both of the cases is beyond the liquidus temperature of the material. At the free edge location, the temperature for the case 11 mm is higher than that for the case of 13 mm, as the heat is absorbed by less material.

To study the behavior of temperature and strain in the weld mushy zone in more detail, a $4 \times 4 \times 1.25$ mm^3 volume is extracted at the weld starting location from the simulation results. The solidus and liquidus temperatures of the studied material are 1670 and 1783 K, respectively. From the simulation results, the isothermal surfaces between the solidus and liquidus temperature show the development of the weld mushy zone. The strain evolution in the weld mushy zone

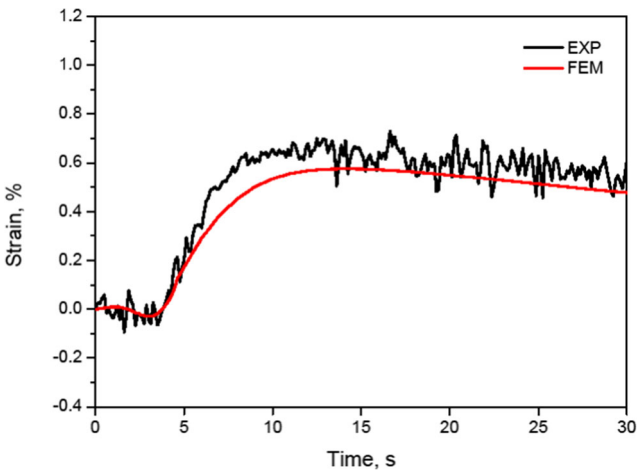

Fig. 6 Strain validation at the free edge in the middle of the weld sheet when welding at 13 mm from the free edge

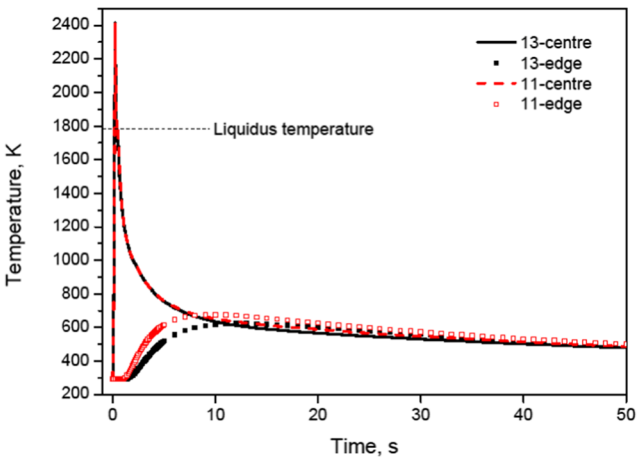

Fig. 8 Simulated temperature evolution located at the starting edge in the weld center and at the free edge when welding at 13 and 11 mm from the free edge

over a period up to 0.5 s after the start of welding is presented in Fig. 9. Welding at 13 mm from the free edge is discussed here. A volumetric heat source is initially applied outside of the starting edge and travels along the weld center line. At 0.2 s after the start of welding, melting at the starting edge is observed as the heat source partially enters the steel sheet. The dimension of the weld pool on the top surface is larger than that on the bottom surface due to the conical heat source applied, which creates a thermal gradient along the thickness direction. A strain of up to 1.4% is observed along the fusion boundary. At 0.25 s, the width of the weld pool has reached the maximum size. At 0.3 s, the center of the heat source has passed the starting edge; the width of the weld pool starts deceasing due to subsequent cooling. A strain of up to 2.6% accumulates at the fusion boundary from the bottom surface, as the bottom surface cools faster than the top surface. From 0.35 to 0.4 s, a tail of the weld pool on the top surface is formed because of the motion of the heat source. The semisolid regions at the weld starting location become larger, and the strains are accumulated in these regions. At 0.44 s, the semisolid regions from both sides of the weld start to coalesce. The strain re-distributes in the weld mushy zone to balance the solidification shrinkage and thermal contraction. From 0.45 to 0.48 s, the weld mushy zone is elongated along the weld center line. The strain gradually decreases when the heat source is moving further into the sheet. A line integration of the temperature between solidus and liquidus along the weld center line is applied, from which the maximum length of the weld mushy zone is calculated to be 0.75 mm. At 0.5 s, the complete mushy zone has passed the weld starting edge. The development of the isothermal surface when welding at 11 mm is almost the same as welding at 13 mm from the free edge, as the temperature histories in the weld center are similar. A maximum strain during solidification is calculated to be 3.2 and 3.6% when welding at 13 and 11 mm from the free edge, respectively. As hot cracking is observed when welding at 11 mm, it is reasonable to expect a larger strain. Therefore, a critical strain of at least 3.2% during solidification can be defined as a safe threshold to guarantee a weld without hot cracking when welding this specific TRIP steel.

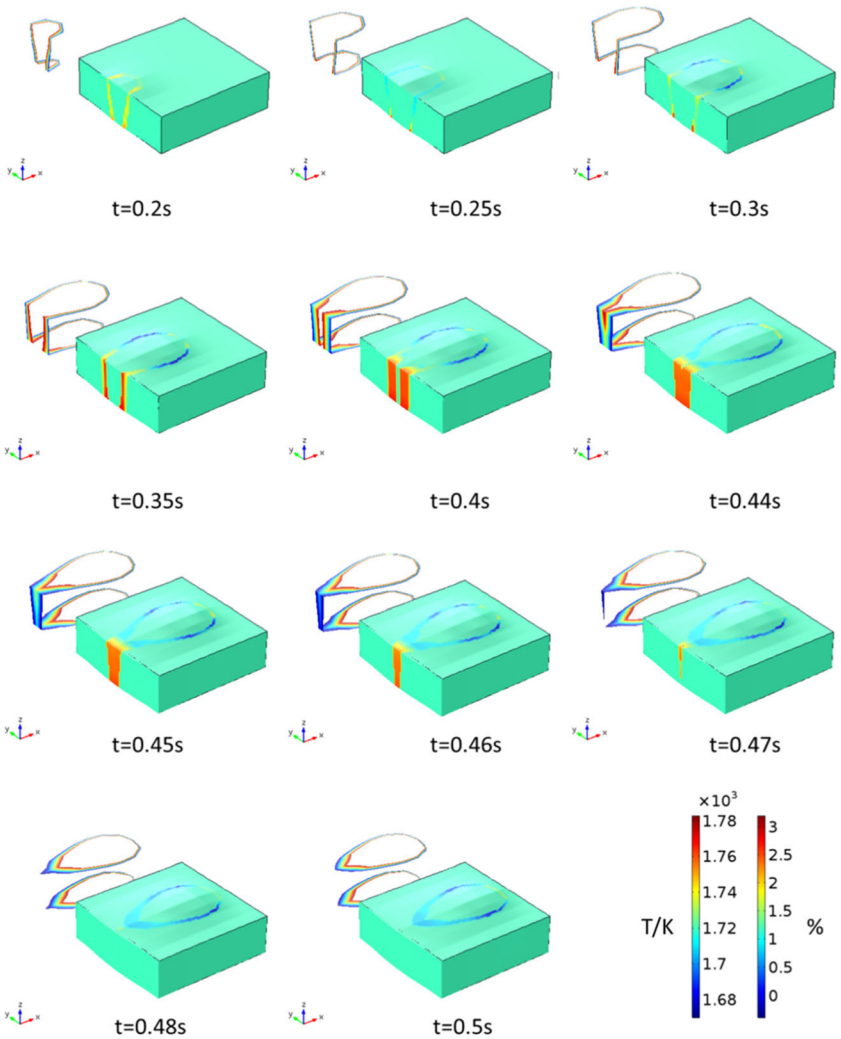

Fig. 9 Development (time from 0.2 to 0.5 s) of isothermal surface and transverse strain evolution in weld mushy zone when welding at 13 mm from the free edge

Two more simulations were carried out using the same FE model to test the hot cracking criterion obtained, (i) welding at 13 mm from the free edge with 10% increment of heat input and (ii) welding at 11 mm from the free edge with 10% reduction of heat input. A maximum strain during solidification is calculated to be 4.6 and 2.5% for the modified cases. Welding at 13 mm with a 10% increment of heat input is expected to result in hot cracking, whereas welding at 11 mm with a 10% reduction of heat input shall not show any cracks. To check the validity of this prediction, two additional welding experiments were carried out, and the prediction of the model proves to be correct, i.e., crack was observed at 13 mm from the free edge, whereas no crack was found at 11 mm from the free edge.

6 Conclusion

In this study, the standard self-restraint hot cracking was modified by welding at various locations parallel to the free edge of a steel coupon, in order to determine a hot cracking criterion of the tested TRIP steel under the same heat input and constraint condition. The crack susceptibility decreases when welding is performed at a larger distance from the free edge.

In situ temperature and strain measurements were carried out using pre-attached thermocouples and digital image correlation, respectively. The experimental arrangement applied in this study is able to measure the transient strain at a distance greater than 3 mm from the weld center line on the top surface during laser welding.

A thermal-mechanical FE model was constructed. A good agreement of transient temperature and strain is achieved between the experimental and numerical results. The FE model described in this study is able to predict the temperature and strain evolution and distribution during welding.

The critical strain for the onset of hot cracking in the TRIP steel examined was found to be in the range of 3.2 to 3.6%.

By increasing the heat input by 10% for the case of 13 mm and decreasing the heat input by 10% for the case of 11 mm, the FE model predicts a reversed cracking susceptibility, which is also experimentally confirmed.

Acknowledgements This research was carried out under project numbers F22.8.13485a and F22.8.13485b in the framework of the Partnership Program of the Materials innovation institute M2i (www.m2i.nl) and the Foundation for Fundamental Research on Matter (FOM) (www.fom.nl), which is part of the Netherlands Organisation for Scientific Research (www.nwo.nl). The authors would also like to thank the industrial partner in this project "Tata Steel Nederland B.V." for the financial support.

References

1. Matlock DK, Speer JG (2009) Third generation of AHSS: microstructure design concepts. In: Haldar A, Suwas S, Bhattacharjee D (eds) Microstructure and texture in steels: and other materials. Springer, London, pp 185–205. https://doi.org/10.1007/978-1-84882-454-6_11
2. Kuziak R, Kawalla R, Waengler S (2008) Advanced high strength steels for automotive industry: a review. Arch Civ Mech Eng 8(2):103–117
3. Larsson JK (2010) Avoidance of crack inducement when laser welding hot-formed car body components—a variable analysis. Phys Procedia 5(Part B):115–124. https://doi.org/10.1016/j.phpro.2010.08.036
4. Aydin H, Essadiqi E, Jung IH, et al (2013) Development of 3rd generation AHSS with medium Mn content alloying compositions. Mat Sci Eng A Struct 564:501–508
5. Bhaduri AK, Srinivasan G, Klenk A, et al (2009) Study of hot cracking behaviour of 14Cr-15Ni-2.5Mo Ti-modified fully austenitic stainless steels using Varestraint and hot ductility tests. Weld World 53(1):17–27
6. Kannengiesser T, Boellinghaus T (2014) Hot cracking tests—an overview of present technologies and applications. Weld World 58(3):397–421
7. Rappaz M, Drezet JM, Gremaud M (1999) A new hot-tearing criterion. Metall Mater Trans A 30(2):449–455
8. Kou S (2015) A criterion for cracking during solidification. Acta Mater 88:366–374
9. Wang L, Wang N, Provatas N (2017) Liquid channel segregation and morphology and their relation with hot cracking susceptibility during columnar growth in binary alloys. Acta Mater 126:302–312
10. Coniglio N, Cross CE (2013) Initiation and growth mechanisms for weld solidification cracking. Int Mater Rev 58(7):375–397
11. Prokhorov NN, Shirshov YV (1974) Effect of welding conditions on character of crack-propagation and load carrying capacity of a welded joint during brittle-fracture of weld metal. Weld Prod 21(6):1–5
12. Clyne TW, Wolf M, Kurz W (1982) The effect of melt composition on solidification cracking of steel, with particular reference to continuous-casting. Metall Trans B 13(2):259–266
13. Yamanaka A, Nakajima K, Yasumoto K, et al (1992) New evaluation of critical strain for internal crack formation in continuous-casting. Rev Metall-Paris 89(7–8):627–633
14. Won YM, Yeo TJ, Seol DJ, et al (2000) A new criterion for internal crack formation in continuously cast steels. Metall Mater Trans B Process Metall Mater Process Sci 31(4):779–794
15. Safari AR, Forouzan MR, Shamanian M (2012) Hot cracking in stainless steel 310s, numerical study and experimental verification. Comput Mater Sci 63:182–190
16. Wang XJ, Lu FG, Wang HP, et al (2016) Micro-scale model based study of solidification cracking formation mechanism in Al fiber laser welds. J Mater Process Technol 231:18–26
17. Ploshikhin V, Prikhodovsky A, Makhutin M, et al (2005) Integrated mechanical-metallurgical approach to modeling of solidification cracking in welds. In: Böllinghaus T, Herold H (eds) Hot cracking

phenomena in welds. Springer Berlin Heidelberg, Berlin, pp 223–244
18. VDEh SEP 1220–3: testing and documentation guideline for the joinability of thin sheet of steel—part 3: Laser beam welding. 2011
19. Agarwal G, Gao H, Amirthalingam M, et al (2017) In situ strain investigation during laser welding using digital image correlation and finite-element-based numerical simulation. Sci Tech Weld Join: 1–6. https://doi.org/10.1080/13621718.2017.1344373
20. Gao H, Hermans MJM, Richardson IM (2013) Simulation of transient force and strain during thermal mechanical testing relevant to the HAZ in multi-pass welds. Sci Technol Weld Join 18(6):525–531
21. Ahmed EAA (2011) Laser welding of advanced high strength steels dissertation RWTH Aachen
22. Gao H, Dutta RK, Huizenga RM, et al (2014) Pass-by-pass stress evolution in multipass welds. Sci Technol Weld Join 19(3):256–264